Comparative Mechanical Microscopy of Mn-Ni-Co 4:1:1 Li-Ion Battery Cathodes

Leon Romano-Brandt, Joris Everaerts, Jinhua Zhou, Bohang Song, Lu Li and Alexander M. Korsunsky, *IAENG Member*

***Abstract* — Mechanical strain phenomena in Li-ion battery cathodes are the pivotal in performance degradation and capacity fading. Two lithium-rich layered Mn-Ni-Co (MNC) cathodes were fabricated with fixed 4:1:1 transition metal cation ratio, but distinctly different microstructures. Cathodes produced based on the mixed oxide powders were incorporated in coin cells and subjected to charge cycling, following which they were extracted and extensively characterised using a multi-technique microscopy approach. The results reveal the correlation between microstructure, stress and durability and point out possible avenues for optimising cathode design to improve the stability of future generation batteries.**

***Index Terms*— Li-ion battery, MNC, Mechanical degradation, Residual Stress**

I. Introduction

LI-ION batteries are used to power most mobile electric appliances and are crucial for the anticipated future growth in electric-powered vehicles. The price of the battery accounts for a large part of the total cost of an electric vehicle, car manufacturers are investigating alternative compositions to replace the cathode materials currently available commercially. Cobalt is one of the most expensive materials in cathodes. However, due to its stabilising effect on the cathode material, it cannot be entirely replaced. in order to ensure robustness, durability and safety of operation of new battery cathode materials, it is vitally important to understand the influence of elemental substitution. Reducing battery prices by reducing the Cobalt content requires thorough investigation.

Much work has been published on the stability of MNC cathode materials with low Co content, however, mostly from an electrochemical point of view [1–3]. As reported previously, the cycling-induced performance degradation in Li-rich MNC materials is intrinsically tied to mechanical degradation phenomena at the pico-, nano- and micro-scale [4–6]. These mechanisms are initiated by the chemical changes in the valence of transition metal ions, that lead to interatomic bond deformation and crystal lattice strain, as demonstrated in a number of recent studies using synchrotron X-ray diffraction, and absorption spectroscopy (XANES and EXAFS). In [7], *operando* battery cycling was performed on a synchrotron instrument at Diamond Light Source to reveal lattice expansion and contraction on the order of 1% during lithiation cycle. This corresponds to the interplanar lattice spacing of ~2.84Å undergoing changes of ~2pm, i.e. pico-scale variation in the interatomic bond lengths. Similar conclusions were drawn in [8] using *operando* spectroscopic analysis.

Pico-scale crystal lattice deformation propagates to the nano-structural level. Structural inhomogeneity and strain anisotropy in active cathode oxide spheroids manifest themselves through Li ion concentration ‘hotspots’ associated with stress concentration, as seen from Focused Ion Beam-Time of Flight – Secondary Ion Mass Spectroscopy (FIB-TOF-SIMS) [9]. These mechanisms can be associated with stress concentration, leading to active material fragmentation at the nano-scale, and the loss of ion conductivity across the cathode.

In this work, we reveal how microstructure, stresses and performance are interlinked, by using a broad variety of advanced characterisation methods such as Scanning Electron Microscopy (SEM), FIB, Electron Backscatter Diffraction (EBSD), Energy-Dispersive X-ray Spectroscopy (EDS), Kernel Average Misorientation (KAM) and the FIB-DIC ring-core method for residual stress evaluation [10]. In addition, we compare two very different cathode microstructure types and analyse how their cycling performance is influenced by their microstructure.

II. Sample Fabrication and Preparation

A. Type I: Layered Li-rich Oxide Cathode: $Li_{1.2}Mn_{0.54}Ni_{0.13}Co_{0.13}0_2$

The synthesis of the active material of $Li(Li_{0.2}Mn_{0.54}Ni_{0.13}Co_{0.13})O_2$ was performed according to the spray-dryer assisted sol-gel method. Metal acetates of Mn, Ni, and Co were dissolved in a 200 mL aqueous solution (0.3 M). The dissolved solution was slowly dripped into a solution of 3% excess amount of lithium acetate and citric acid as a chelating agent with the identical stoichiometry as

Manuscript received March 20, 2018; revised April 11, 2018.

León Romano-Brandt is with MBLEM, the University of Oxford, Department of Engineering Science, Oxford OX1 3PJ, phone: +44 (0) 1865 283 447; e-mail: leon.romanobrandt@eng.ox.ac.uk

Joris Everaerts is with MBLEM, the University of Oxford, Department of Engineering Science, Oxford OX1 3PJ, e-mail: joris.everaerts@eng.ox.ac.uk

Jinhua Zhou is with the Department of Mechanical Engineering, National University of Singapore, 9 Engineering Drive 1, EA#07-08, Singapore, 117575, e-mail: e0168727@u.nus.edu

Bohang Song is with Oak Ridge National Laboratory, P.O. Box 2008, Oak Ridge, TN 37831, USA, e-mail: songb@ornl.gov

Lu Li is with the Department of Mechanical Engineering, National University of Singapore, 9 Engineering Drive 1, EA#07-08, Singapore, 117575, e-mail: luli@nus.edu.sg

Alexander M. Korsunsky is Head of MBLEM, the University of Oxford, Department of Engineering Science, Oxford OX1 3PJ; e-mail: alexander.korsunsky@eng.ox.ac.uk

the metal ions, while stirring continuously. This solution was dried by a spray-dryer (YC-015, Shanghai Politech Instrument & Equipment Co. Ltd) and further drying was carried out on the as-sprayed precursor at 80 °C overnight. Drying was followed by the calcination at 800 °C for 15 h at a heating rate of 5 °C min^{-1}. The powders were cooled down in air after calcination. The electrode slurry was prepared by mixing $Li(Li_{0.2}Mn_{0.54}Ni_{0.13}Co_{0.13})O_2$ powder, carbon black and polyvinylidene fluoride (PVDF) with the weight ratio of 80 : 10 : 10, respectively, in the n-methyl-2-pyrrolidone (NMP) solution. The mixture was constantly stirred overnight to obtain homogenous dispersion. The prepared slurry was pasted onto aluminium foil and dried at 120 °C overnight, prior to cutting into working electrode circular pieces with 12 mm diameter. Coin half-cells were assembled with the working electrode (cathode), Li-foil (anode) and two pieces of separator (Celgard 2500). For the electrolyte, 1 M $LiPF_6$ in EC: DEC=1:1 organic solution was used. The diameter and thickness of coin cells were 20 mm and 2.5 mm, respectively. Subsequently, cells were cycled 10 and 100 times, respectively, at a charge/ discharge current of 0.2C, with 1C = 250 mA g^{-1}. After disassembling the cells, the cathodes were dried for characterisation.

B. *Type II: $Li_{1.2}Mn_{0.53}Ni_{0.13}Co_{0.13}0_2$*

The layer lithium-rich oxide $Li_{1.2}Mn_{0.53}Ni_{0.13}Co_{0.13}O_2$ cathode material was synthesized by the common sol-gel method. Firstly, metal salts were dissolved in deionized water: $C_6H_8O_7$ was followed by $LiAc.2H_2O$, $MnAc_2.4H_2O$, $NiAc_2.4H_2O$ and $CoAc_2.4H_2O$. Thereafter, NH_4OH was added dropwise in order to adjust the PH value to 7. A gel was formed by simultaneously stirring and drying the solution with an agitator at 80°C. In a second step, the mixture was pre-calcined at 450°C for 4 hours in air, which was hen ground into powder and pressed into tablets. These tablets were then calcined again at 900°C for 12 hours in air. Samples with 10 and 100 charge/ discharge cycles were produced with charge/ discharge rates of 0.2 and 0.4C. After disassembling the cells, the cathodes were dried for characterization.

III. Functional Sample Analysis

A. *FIB Sectioning, SEM imaging and EDS characterisation*

FIB sectioning at 30 keV beam energy and beam current of 0.17 nA with subsequent SEM imaging combined with EDS analysis at 10 keV was performed using a TESCAN LYRA 3 instrument. The analysis revealed significant differences in microstructure between Type I and Type II samples. While Type I material consists of distinct, approximately spherical oxide particles (green) embedded in a matrix of polymer binder containing carbon black (Figure 1, red), Type II material exhibits finely dispersed active material regions (Figure 2).

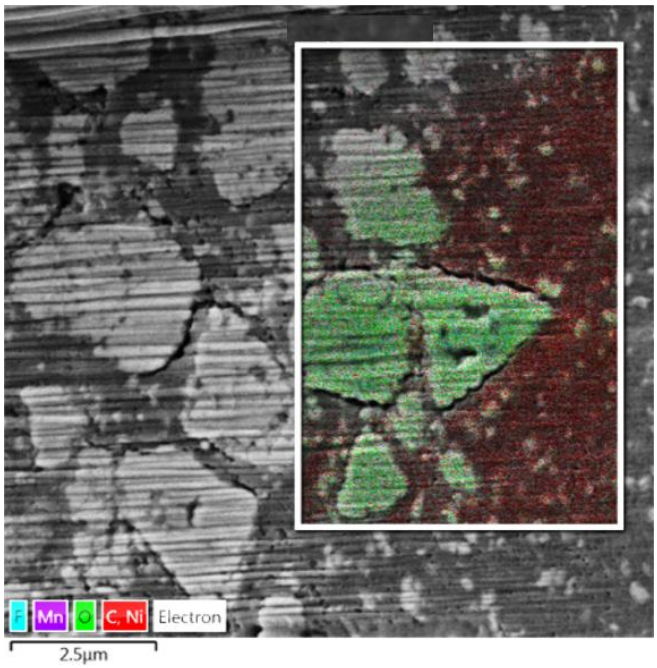

Figure 1. Microstructure of Type I sample FIB section after 10 charging cycles (10+ state)

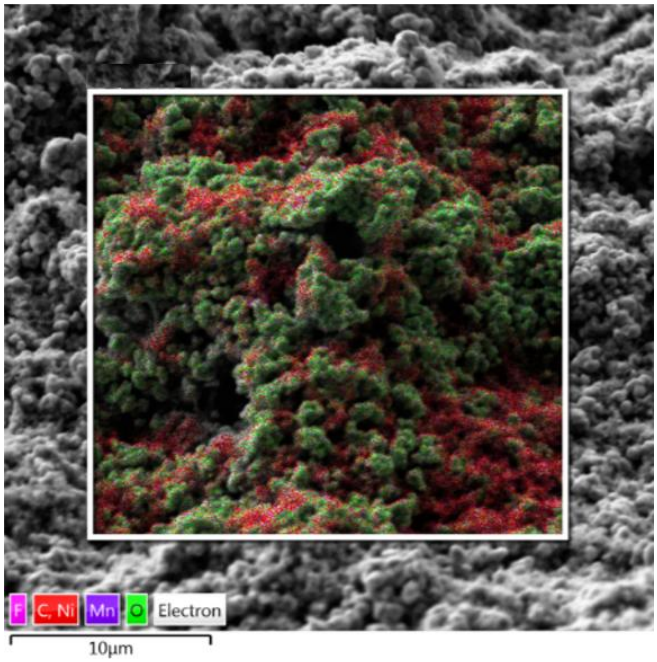

Figure 2. Microstructure of Type II sample FIB section in pristine discharged cathode (0- state).

B. *EBSD Mapping and KAM analysis (Type I)*

EBSD mapping allows for determining the grain orientation of the oxide particles composing the spheroids by analysis of Kikuchi patterns. The EBSD maps were acquired at an electron beam energy of 15 keV. Figure 3 shows the grain orientation map for Type I active material. The inverse pole figure map (bottom right, reference direction z) shows red, green and blue areas, which can respectively be identified as <100>, <110>, and <111> oriented grains.

ISBN: 978-988-14048-9-3
ISSN: 2078-0958 (Print); ISSN: 2078-0966 (Online)

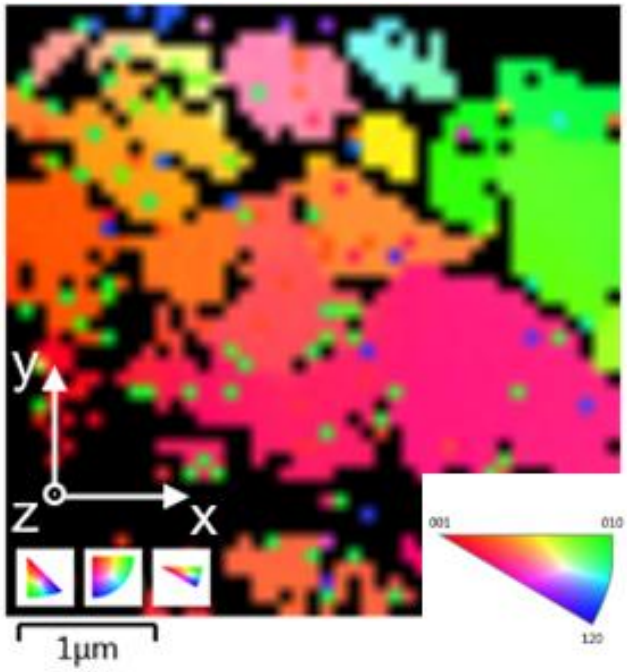

Figure 3. EBSD Map of Type I sample after 10 charging cycles (10+ state) clearly showing the orientation of individual grains.

By post-processing the acquired Kikuchi patterns, it is possible to determine the misorientation angles of grain boundaries. This analysis, named Kernel Average Misorientation [11], can be used to qualitatively estimate the mismatch strain at grain boundaries. The result for the Type I sample is shown on Figure 4. It can be clearly seen that the grain boundaries show significant misorientation.

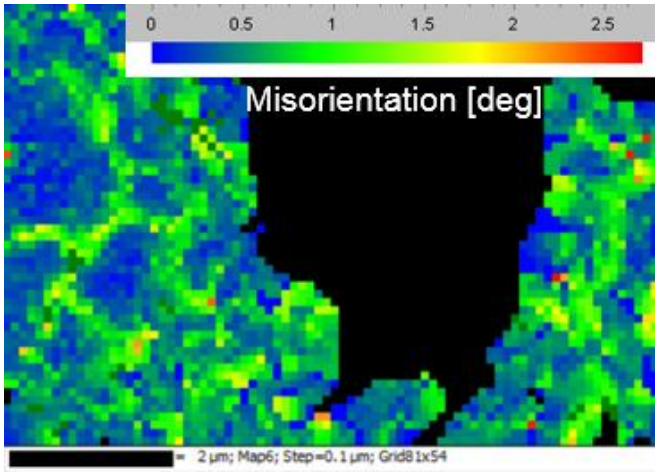

Figure 4. KAM map of Li rich Oxide (coloured) colour-coded according to magnitude of grain misorientation angle. The carbon-polymer matrix is shown in black.

C. Nano-indentation

In order to determine the elastic mechanical properties of Type II samples, in-SEM nano-indentation was performed using a cube-corner indenter tip with a maximum load of 3 mN. This allows for the precise placement of the indentation location on the surface. From the resulting load-displacement curve the hardness and Young's modulus were determined using the Oliver-Pharr method [12]. Due to the fine grains of the active material, the determined properties are average bulk properties for the matrix-spheroid-composite. The hardness was determined to be 0.9 GPa, whereas the Young's modulus was calculated to be E = 3.6 GPa.

D. FIB-DIC Ring-Core Method

The FIB-DIC Ring-Core method is a flexible and powerful tool for profiling and mapping absolute residual stress values at the micron scale. Flexible ring-core diameters between ~2-20 µm allow probing different depths. To obtain a local stress value, the following steps are required [10]: firstly, a ring-core is being milled step-wise into the location, at which the residual stress is aimed to be determined. The diameter of the ring-core was chosen to be 10 µm in order to guarantee sufficient averaging of both active and matrix material (Figure 5). In between the milling steps, high resolution SEM frames are being acquired at a surface-sensitive beam energy of 5 keV. After the acquisition, a MATLAB-based Digital Image Correlation tool (Eberl, 2010) is being used to track the displacement of surface points. From the slope of the displacement versus position plot, it is possible to calculate the relaxation strain profiles, which are then being fitted to a FEM-based theoretical function. From the complete elastic strain relief values $\Delta\varepsilon^{\infty}$ it is then possible to calculate the residual stresses in the two principle directions σ_{xx} and σ_{yy}. By applying Hooke's law, the residual stress can be calculated as follows:

$$\sigma_{xx} = -\frac{E}{(1-\nu^2)}\left[\Delta\varepsilon_{xx}^{\infty} + \nu\Delta\varepsilon_{yy}^{\infty}\right]$$

$$\sigma_{yy} = -\frac{E}{(1-\nu^2)}\left[\Delta\varepsilon_{yy}^{\infty} + \nu\Delta\varepsilon_{xx}^{\infty}\right]$$

For the analysed Type I cathode, the Young's modulus obtained from nano-indentation was used. The Poisson's ratio was assumed to be ν = 0.34, based on existing PVDF data [13]. For Type I samples, which were cycled at 0.2C, the residual stresses are summarised below, in Table 1.

TABLE I
RESIDUAL STRESSES FROM FIB-DIC RING-CORE TECHNIQUE

Sample state	Residual Stress [MPa]
Pristine discharged (0-)	48
One charge cycle (1+)	65
100 charge cycles (100+)	σ_{xx} = 59, σ_{yy} = 30

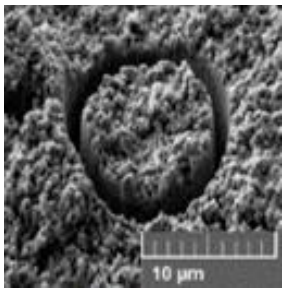

Figure 5: 10 µm ring-core on Type I cathode material for residual stress evaluation

ISBN: 978-988-14048-9-3
ISSN: 2078-0958 (Print); ISSN: 2078-0966 (Online)

The residual stress values for the Pristine discharged battery were obtained by averaging two different samples, which showed a large difference in residual stress (35 vs 60 MPa). This is expected to be associated with the sample preparation method, which includes drying of the electrolyte. However, all other measurements were highly consistent, varying by at most ±5 MPa for the 1+ state samples. Each of the measured samples showed highly equi-biaxial stress behaviour, leading to only one stress value. In the case of the 100+ state cathode, however, biaxial cracking was observed, which indicates biaxial tension beyond the fracture strain. This as such is a significant observation, as it represents an important mechanism for the degradation of cathode material after cycling. As this fracture highly distorts the stress field, the xx and yy components of residual stress were found to be very different from each other, and are therefore mentioned separately in Table 1. A picture of the biaxial fracture pattern is shown on Figure 6.

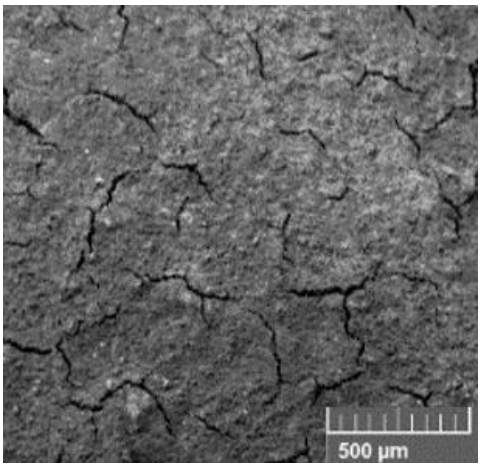

Figure 6. Biaxial fracture of the Type I cathode after 100 charging cycles (100+ state)

IV. Results and Discussion

Two different microstructures of Type I and Type II Mn:Ni:Co (4:1:1) were presented and analysed by various techniques. Although similar fabrication routes were used for both types – namely, sol-gel and spray drying – significant microstructural differences were found, as confirmed by the above-presented FIB-SEM and EDS data. While Type I samples contained clearly identifiable spheroid oxide particles enclosed in a carbon/polymer matrix, Type II samples showed a fine dispersion of the Li-rich active material. These differences clearly have a pronounced effect on charge rate capability and durability of cathodes, which highlights the importance of establishing tight relationships between structure, stress and performance in these systems.

EBSD analysis of the grain orientation within secondary particles of Type I active MNC material revealed misorientation that exerts a strong influence on the deformation behaviour through misfit strain, arising during discharge cycling. We suggest that this misfit arises due to the anisotropy of expansion and contraction due to lithiation. Post-processing of EBSD data for KAM analysis revealed a high degree of lattice disorder at grain boundaries, which was inherited from the process of secondary particle fabrication.

In order to obtain the elastic mechanical properties of the material for the FIB-DIC ring-core technique, nano-indentation was employed. The in-SEM nano-indentation allowed the determination of the average hardness and Young's modulus of the fine-grained Type I material.

These results were used to calculate the residual stresses of the cathode materials as a function of the state of charge cycling. Although the data contains a certain amount of insecurity due to the sample preparation methods, a clear trend of increasing tensile residual stress is visible, which results in the biaxial fracture of the cathode material, as shown on Figure 6.

In summary, it was shown that small deviations in manufacturing parameters can entirely change the resulting microstructure of the cathode material. Multi-technique characterisation revealed a clear link between microstructure, stress and degradation of the MNC cathodes. Based on these results, further investigation can be launched in order to optimise the grain structure and residual stress to avoid degradation during cycling.

Acknowledgements

The authors wish to express their gratitude to Dr Vedran Glavas, Volkswagen Group Research, Materials and Manufacturing Methods, Volkswagen Group, Brieffach 011/14990, 38436 Wolfsburg, Germany, e-mail: vedran.glavas@volkswagen.de, for expert advice that greatly assisted progress in the reported study.

References

[1] R. Jung, M. Metzger, F. Maglia, C. Stinner, H.A. Gasteiger, Oxygen Release and Its Effect on the Cycling Stability of $LiNi_x Mn_y Co_z O_2$ (NMC) Cathode Materials for Li-Ion Batteries, J. Electrochem. Soc. 164 (2017) A1361–A1377. doi:10.1149/2.0021707jes.

[2] M. Dixit, B. Markovsky, F. Schipper, D. Aurbach, D.T. Major, Origin of Structural Degradation during Cycling and Low Thermal Stability of Ni-Rich Layered Transition Metal-Based Electrode Materials, J. Phys. Chem. C. 121 (2017) 22628–22636. doi:10.1021/acs.jpcc.7b06122.

[3] J. Yang, M. Hou, S. Haller, Y. Wang, C. Wang, Y. Xia, Improving the Cycling Performance of the Layered Ni-Rich Oxide Cathode by Introducing Low-Content Li2MnO3, Electrochim. Acta. 189 (2016) 101–110. doi:10.1016/j.electacta.2015.12.080.

[4] G. Sun, T. Sui, B. Song, H. Zheng, L. Lu, A.M. Korsunsky, On the fragmentation of active material secondary particles in lithium ion battery cathodes induced by charge cycling, Extrem. Mech. Lett. 9 (2016) 449–458. doi:10.1016/j.eml.2016.03.018.

[5] A.M. Korsunsky, T. Sui, B. Song, Explicit formulae for the internal stress in spherical particles of active material within lithium ion battery cathodes during charging and discharging, Mater. Des. 69 (2015) 247–252. doi:10.1016/j.matdes.2014.12.058.

[6] B. Song, T. Sui, S. Ying, L. Li, L. Lu, A.M. Korsunsky, Nano-structural changes in Li-ion battery cathodes during cycling revealed by FIB-SEM serial sectioning tomography, J. Mater. Chem. A. 3 (2015) 18171–18179. doi:10.1039/C5TA04151A.

[7] B. Song, S.J. Day, T. Sui, L. Lu, C.C. Tang, A.M. Korsunsky, Mitigated phase transition during first cycle of a Li-rich layered cathode studied by in operando synchrotron X-ray powder diffraction, Phys. Chem. Chem. Phys. 18 (2016) 4745–4752. doi:10.1039/C5CP04801J.

ISBN: 978-988-14048-9-3
ISSN: 2078-0958 (Print); ISSN: 2078-0966 (Online)

[8] T. Kim, B. Song, A.J.G. Lunt, G. Cibin, A.J. Dent, L. Lu, A.M. Korsunsky, Operando X-ray Absorption Spectroscopy Study of Atomic Phase Reversibility with Wavelet Transform in the Lithium-Rich Manganese Based Oxide Cathode, Chem. Mater. 28 (2016) 4191–4203. doi:10.1021/acs.chemmater.6b00522.

[9] T. Sui, B. Song, J. Dluhos, L. Lu, A.M. Korsunsky, Nanoscale chemical mapping of Li-ion battery cathode material by FIB-SEM and TOF-SIMS multi-modal microscopy, Nano Energy. 17 (2015) 254–260. doi:10.1016/j.nanoen.2015.08.013.

[10] A.J. Lunt, N. Baimpas, E. Salvati, I.P. Dolbnya, T. Sui, S. Ying, H. Zhang, A.K. Kleppe, J. Dluhoš, A.M. Korsunsky, A state-of-the-art review of micron-scale spatially resolved residual stress analysis by FIB-DIC ring-core milling and other techniques, J. Strain Anal. Eng. Des. 50 (2015) 426–444. doi:10.1177/0309324715596700.

[11] R.R. Shen, P. Efsing, Ultramicroscopy Overcoming the drawbacks of plastic strain estimation based on KAM, Ultramicroscopy. 184 (2018) 156–163. doi:10.1016/j.ultramic.2017.08.013.

[12] W.C. Oliver, G.M. Pharr, An improved technique for determining hardness and elastic modulus using load and displacement sensing indentation experiments, J. Mater. Res. 7 (1992) 1564–1583. doi:10.1557/JMR.1992.1564.

[13] K. Takahashi, K. Higa, S. Mair, M. Chintapalli, N. Balsara, V. Srinivasan, Mechanical Degradation of Graphite/PVDF Composite Electrodes: A Model-Experimental Study, J. Electrochem. Soc. 163 (2016) A385–A395. doi:10.1149/2.0271603jes.

ISBN: 978-988-14048-9-3
ISSN: 2078-0958 (Print); ISSN: 2078-0966 (Online)